# Modelling of transition from upper to lower bainite in multi-component system

L. Guo[a,*], H. Roelofs[b], M. I. Lembke[c], H. K. D. H. Bhadeshia[a]

[a]*Department of Materials Science and Metallurgy, University of Cambridge, 27 Charles Babbage Road, Cambridge CB3 0FS, U.K.*

[b]*R& D, Swiss Steel AG, Emmenweidstr. 90, CH-6020 Emmenbrcke, Switzerland*

[c]*Steeltec AG, Emmenweidstr. 72, CH-6020 Emmenbrcke, Switzerland*

**Abstract**

A model for estimating the upper to lower bainite transition has been developed for the iron-carbon-manganese-chromium-silicon alloy system by comparing the time required to decarburise a supersaturated bainitic ferrite platelet and that needed for the start of cementite precipitation in the ferrite. The problem is treated as a competition between the decarburisation time and the kinetics of cementite precipitation. Lower bainite is induced when the latter process is faster. The time for forming a volume fraction of 0.01 of the equilibrium amount of cementite is taken as the precipitation start time. The model was calibrated using experimental data from iron-carbon system, and verified with iron-carbon-manganese-molybdenum system and an experimental steel currently being developed for high-strength applications.

*Keywords:* Upper bainite, Lower bainite, Transition temperature, Cementite, Decarburisation

## 1. Introduction

The microstructure of bainite consists of a non-lamellar mixture of ferrite and carbides, which can be classified further into upper and lower bainite

*Corresponding author

*Email address:* lg446@cam.ac.uk,lei-guo@outlook.com (L. Guo)

depending on the details of carbide precipitation [1]. The mechanism of the formations of these two different morphologies is illustrated in Fig. 1, in upper bainite the partitioning of carbon from supersaturated ferrite into the residual austenite is so rapid that the cementite precipitates from the austenite, between the ferrite plates. In the case of lower bainite, which forms at relatively low temperature, the carbides precipitate due to the tempering of the supersaturated ferrite plates, with less carbon partitioning into the austenite so that precipitation from austenite is more limited [1]. The model, for Fe-C steels, was quantitatively expressed by Takahashi and Bhadeshia [2, 3] based on a comparison of the decarburisation and precipitation times. Cementite precipitation was modelled using Avrami equation with kinetic data fitted from hardness changes during the early stages of tempering of martensite. Ławrynowicz [4] applied this model to a Fe-0.38C-0.29Si-0.63Mn-0.93Cr wt % steel, using exactly the same Avrami equation for cementite precipitation kinetics due to the identical hardness change during tempering compared with plain carbon steel with 0.39 C wt %. Azuma et al. [5] developed a simultaneous transformation model including the bainite transformation, and cementite precipitation from ferrite and austenite. The nucleation density and interfacial energy were obtained by fitting to experimental data.

Alloying elements can affect the kinetics of cementite precipitation substantially. Silicon is well known to retard cementite precipitation [6–12]. Cr and Mn both can retard the coarsening of cementite particles in the latter stage of tempering of martensite [13–15], but their effects on the early stage of cementite precipitation is not clear. The purpose of this study is to extend the model developed by Takahashi and Bhadeshia to include the solutes Mn, Si and Cr, and apply the results to a wide variety of steels.

## 2. Experimental procedure

A steel provided by Swiss Steel AG was used to validate the model, (Table 1). Cylindrical samples of diameter 8 mm, length 10 mm were machined from the mid-radius position of a steel bar of diameter 32 mm. Heat treatment was carried out in a THERMECMASTER-Z thermomechanical simulator. Samples were heated to 950 °C at a rate of 5 °C $s^{-1}$, held at this temperature for 5 min, then cooled to the isothermal soaking temperature of 400 °C, 370 °C and 340 °C at a rate of 10 °C $s^{-1}$, soaked for 1 h before cooling to ambient temperature.

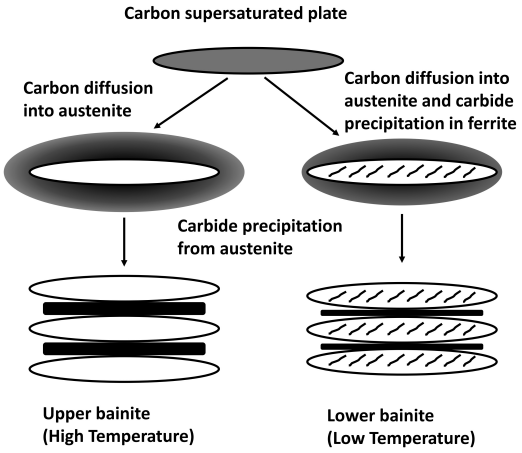


Figure 1: Schematic illustration of upper and lower bainite formation, following Takahashi and Bhadeshia [2]

The $M_s$ was measured using a 8 mm diameter hollow sample with a hole of diameter 5 mm, quenched at a rate of $40\,^{\circ}\mathrm{C\,s^{-1}}$, and found to be $343 \pm 8\,^{\circ}\mathrm{C}$. The $B_s$ was measured by isothermal transformation at different temperatures, and was determined to be $500 \pm 10\,^{\circ}\mathrm{C}$.

To investigate precipitation, thin foils for transmission electron microscopy (TEM) were prepared using a twin-jet electro-polisher set at a voltage of 27 V, with the electrolytic solution consisting of 5 vol % perchloric acid, 25 vol % glycerol and 70 vol % ethanol. The temperature of the solution during thinning was maintained at $6\,^{\circ}\mathrm{C}$. TEM investigation was carried out on a JOEL 200CX transmission electron microscope operating at 200 kV.

Table 1: Chemical composition of alloy (wt %).

| C | Si | Mn | Ni | Mo | Cr | Cu | S |
|---|---|---|---|---|---|---|---|
| 0.224 | 1.0 | 1.542 | 0.086 | 0.141 | 1.54 | 0.168 | 0.146 |

## 3. Decarburising of supersaturated bainite subunits

The time required to decarburise a supersaturated bainite subunit is given by [2, 16, 17]

$$\frac{w_\alpha}{2}(\bar{x} - x^{\alpha\gamma}) = \int_0^\infty [x_\gamma \{z, t_d\} - \bar{x}]dz \tag{1}$$

where $t_d$ is the decarburising time, $w_\alpha$ is the thickness of the bainite subunit, $\bar{x}$ is the nominal carbon content of the alloy, $x^{\alpha\gamma}$ and $x^{\gamma\alpha}$ are the carbon content of ferrite and austenite at the interface where they are in paraequilibrium, $z$ is the coordinate whose origin is defined at the $\gamma/\alpha$ interface and positive in austenite. The left side of equation is the amount of carbon being partitioned out from the ferrite plate, on the right side is the amount of carbon enrichment in austenite. Because carbon can diffuse out from both broad surfaces of the ferrite plate, only half thickness of the plate needs to be considered.

Carbon diffuses much faster in ferrite than in austenite at the same temperature [18], so it is reasonable to assume that the decarburisation process is controlled by diffusion in austenite. Thus, the carbon concentration in austenite can be given by the Van-Ostrand-Dewey solution to Fick's second law as follows [19]:

$$x_\gamma \{z, t_d\} = \bar{x} + (x^{\gamma\alpha} - \bar{x})\text{erfc}\left\{\frac{z}{2\sqrt{Dt_d}}\right\} \tag{2}$$

where $D$ is the carbon diffusivity in austenite.

On combining the Eq.1 and 2, the decarburisation time is [1]

$$t_d = \frac{\pi w_\alpha^2 (\bar{x} - x^{\alpha\gamma})^2}{16D(x^{\gamma\alpha} - \bar{x})^2} \tag{3}$$

The carbon diffusivity in austenite is a function of the carbon concentration only[20–22]; its dependence on substitutional solute content is relatively weak [16]. It is necessary to use the weighted average diffusivity given by [23]

$$\bar{D} = \int_{\bar{x}}^{x^{\gamma\alpha}} \frac{D}{(x^{\gamma\alpha} - \bar{x})} dx \tag{4}$$

[1] The equation in Ref. [2] has a typographical error, where the power of 2 in the denominator $(x^{\gamma\alpha} - \bar{x})^2$ has been omitted.

The carbon diffusivity is calculated using the method in Ref [16].

The calculated effects of alloying elements on the decarburisation of supersaturated ferrite plate are shown in Fig. 2. In the bainite temperature range of interest, as expected, an increase in C content leads to larger decarburisation times ($t_d$). Greater Cr and Mn contents also increase $t_d$, while Si has little effect.

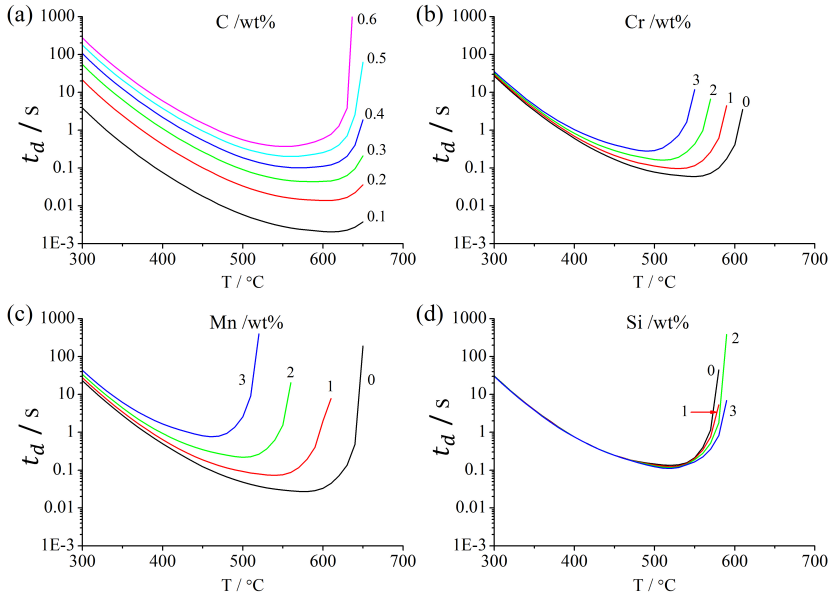


Figure 2: Effect of alloying elements on the decarburisation time ($t_d$) of a supersaturated ferrite plate of 0.2 µm thickness. The numbers next to the lines are elements contents in wt%. Alloying element contents were kept the same as the steel studied (Table 1) except the one under investigation which was varied systematically.

The effects of alloying elements occur through their influences on the paraequilibrium $\gamma/\alpha$ interface composition. Fig. 3 shows the effects of Cr, Mn and Si on the $x^{\alpha\gamma}$ and $x^{\gamma\alpha}$, the $x^{\alpha\gamma}$ is extremely low and is not much affected by the solutes, while $x^{\gamma\alpha}$ is affected substantially, Cr and Mn both reduces $x^{\gamma\alpha}$ at all temperatures, and Mn has a bigger effect. Si does not change $x^{\gamma\alpha}$ much. So an increase in Cr or Mn will decreases $x^{\gamma\alpha}$, hence increases $t_d$.

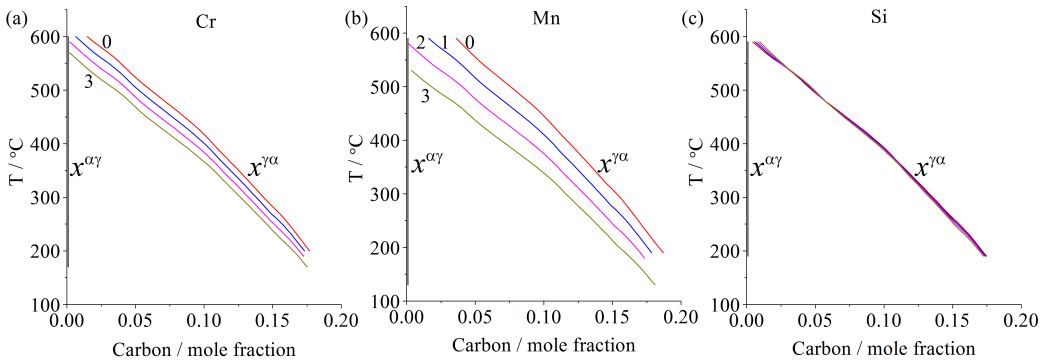


Figure 3: Effects of substitutional solutes on the paraequilibrium $\gamma/\alpha$ interface composition.

## 4. Cementite precipitation

There are evidences that cementite precipitates under paraequilibrium condition in the early stage of tempering of martensite and bainite [24–31], or during bainite transformation [32]. So the kinetics of cementite precipitation was modelled under paraequilibrium condition, using MatCalc version 5.52 [33] with thermodynamic database 'mc_steel' and diffusion database 'mc_sample_fe'. The time for a cementite fraction of 0.01 of its equilibrium quantity is used to define the start time $t_\theta$. The carbon concentration was varied from 0.1 to 0.8 wt% with a step size of 0.1 wt%, Si, Mn and Cr from 1 to 3 wt% in steps of 0.5 wt%, and temperature from 300 °C to 650 °C with 50 °C intervals for calculation purposes. The base composition was otherwise that listed in Table 1.

Cementite was assumed to nucleate heterogeneously on dislocations in the ferrite matrix, but the nucleation site density was determined by fitting the calculated results with the original work of Takahashi and Bhadeshia [2] for the Fe-C system, to reproduce their finding that only upper bainite forms for steels with $\bar{x} < 0.32$ wt%, only lower bainite with $\bar{x} > 0.4$ wt%, and upper or lower bainite depending on the transformation temperature with $0.32 \leq \bar{x} \leq 0.4$ wt%. This gave an effective dislocation density of $5.5{\times}10^6$ m$^{-2}$, which is much lower than reported experimental values, but as not all dislocations are effective nucleation sites, so it maybe a reasonable assumption.

The resulting relations between precipitation start times and alloy element contents and temperatures are very complex and non-linear. The neural

network method was therefore used to represent the calculated data including alloy composition, temperature and cementite precipitation start time as the variables. The method due to MacKay [34, 35] is within a Bayesian framework, which allows the estimation of modelling uncertainty and noise in the data, although the latter is not relevant in the present work since the inputs are calculated. 887 data were obtained from MatCalc, and the dataset was randomised and divided into two groups, one group was used to train the neural network, while the other was used to test its generalisation. The details of the method are described elsewhere [36–38], but the goal is to choose an optimum model which does not over- or under-fit the data. The optimum model complexity is that gives minimum error on the unseen data. Fig. 4 compares the neural network predictions against the MatCalc results. Good agreement was obtained, but there are some outliers associated with big error bars [2].

Figs. 5 and 6 show the alloying element effects on cementite precipitation start time for carbon contents of 0.2, and 0.8 wt% at 400 °C, respectively. The horizontal lines in all figures are $t_\theta$ values for alloy of the same carbon content but without any substitutional alloying element. Each figure is calculated by varying the relevant element content while keeping the other elements as in Table 1. As can be seen for 0.2 wt% carbon, an increase in Cr content leads to a small increase in cementite precipitation time, Mn has the opposite effect, while Si dramatically retards the cementite precipitation at a concentration higher than 2 wt%, though higher temperature leads to faster cementite precipitation. Si is known to retard cementite precipitation from austenite, but the retarding effect is much smaller when precipitation occurs from ferrite since the driving force for precipitation is then much greater [12]. With the increase of carbon content the driving force for cementite precipitation becomes large, leading to fast precipitation, and the effects of substitutional solutes become weak. For 0.8 wt% carbon, even 3 wt% of Si could not effectively slow down cementite precipitation, Fig. 6(c).

Increase in Cr content leads to longer decarburisation times, but it also increases the precipitation start times, so its effect on the transition temperature is not significant. Higher Mn content increases decarburisation time,

[2]The error bars represent uncertainty in the fitting parameters which were obtained by calculating a distribution of sets of weights instead of a unique set of weights. Big error bar means large uncertainty, which is the result of lack of data in the input dataset.

but hastens precipitation, and hence promotes lower bainite. Si has very little effect on decarburisation time but strongly retards cementite precipitation, thus favouring upper bainite. Increased carbon content increases the decarburisation time, and decreases cementite precipitation time (compare Fig. 6 with Fig. 5), so it encourages lower bainite formation.

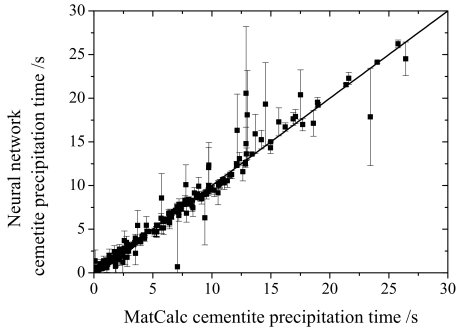


Figure 4: Agreement of neural network predicted $t_\theta$ with MatCalc modelling data.

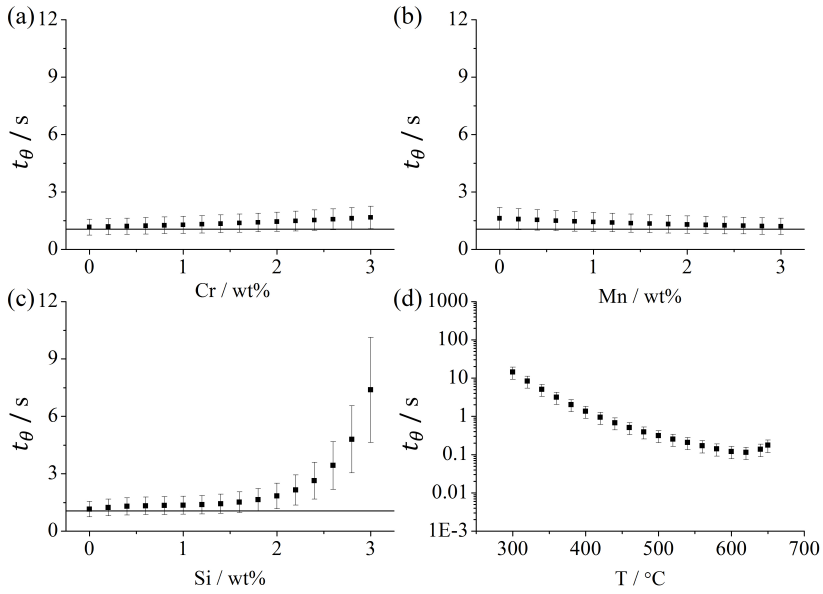


Figure 5: Predicted alloying element and temperature effects on $t_\theta$ for 0.2 wt% of carbon alloy at 400 °C. The horizontal line is the $t_\theta$ for alloy without substitutional alloying element. (a) to (c) are element effects, (d) is the temperature effect.

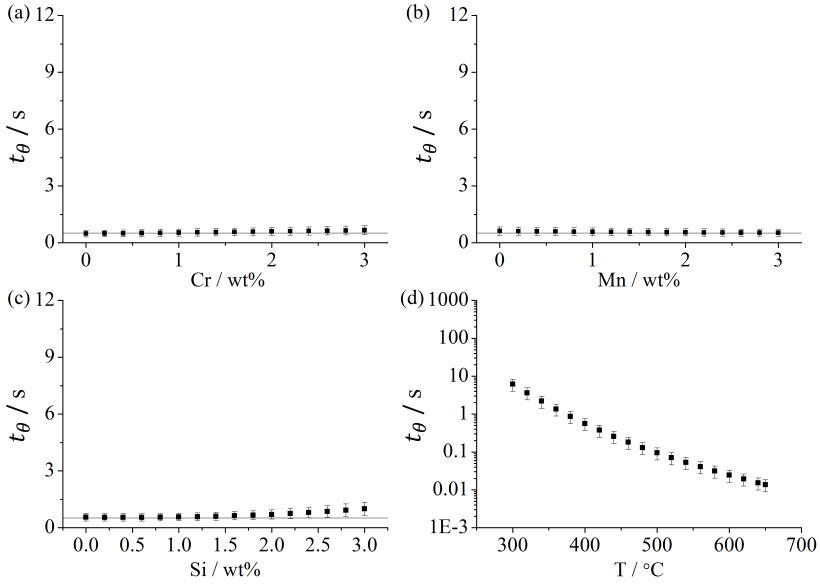


Figure 6: Predicted alloying element and temperature effects on $t_\theta$ for 0.8 wt% of carbon alloy at 400 °C. The horizontal line is the $t_\theta$ for alloy without substitutional alloying element. (a) to (c) are element effects, (d) is the temperature effect.

## 5. Model verification

The time to decarburise a plate must increase with its thickness, thus giving a greater opportunity for cementite to precipitate from supersaturated ferrite. It is expected therefore, that the temperature for the transition to lower bainite is increased as the platelets become thicker. This is illustrated in Fig. 7 for 0.1, 0.2 and 0.3 μm plate thicknesses, and $t_\theta$ for the experimental steel. As expected thickness of 0.1 μm leads to fastest decarburisation, which favours the formation of upper bainite.

### *5.1. Fe-C binary system*

The thickness of bainite subunit is typically about 0.2 μm [1], although it does depend on the strength of austenite and the driving force accompanying the transformation [39]. However, for the present purposes we assumed, thickness $w_\alpha = 0.2$ μm to calculate the decarburisation time. The calculated values of $t_d$ and $t_\theta$ for plain carbon steels as a function of carbon and temperature are shown in Fig. 8, together with the experimental bainite-start ($B_s$)

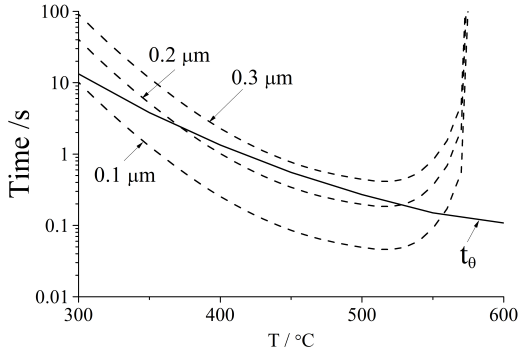


Figure 7: Effect of bainite platelet thickness and cementite fraction on the transition temperature.

and martensite-start ($M_s$) temperatures. As expected the higher the carbon content, the longer the time needed to decarburise the bainite plate, but cementite precipitation is accelerated. For the upper to lower bainite transition, the temperature range of interest is between $B_s$ and $M_s$. As shown in Fig. 8 (a) for carbon content below 0.3 wt%, $t_d$ is always smaller than $t_\theta$ in this temperature range, which means only upper bainite can be obtained, on the other hand, for carbon content higher than 0.4 wt%, only lower bainite will form, as shown in Fig. 8 (b). The calculated lower bainite-start temperature ($LB_s$) for plain carbon steel is show in Fig. 9 against carbon content, it suggests both upper and lower bainite can be obtained for carbon content between 0.32 wt% and 0.4 wt% depending on the transformation temperature. The $LB_s$ increase with carbon content at low carbon content, reaches a peak temperature at about 0.4 wt% of carbon, after that because only lower bainite can be obtained, so the $LB_s$ is effective the $B_s$, which decreases gradually with increasing carbon content. These calculations essentially reproduce the work by Takahashi and Bhadeshia, but using MatCalc for precipitation kinetics. The theory is consistent with experimental data from literature. Oka and Okamoto [40] found there is no upper bainite in plain carbon steels when $x > 0.8$ wt%, while Ohmori and Honeycombe [41] proves no lower bainite could be obtained in steels with $x < 0.4$ wt%, although their observation of upper bainite in steels having carbon concentrations up to 0.85 wt% is not consistent with the theory, nor with the data reported by Oka and Okamoto [40].

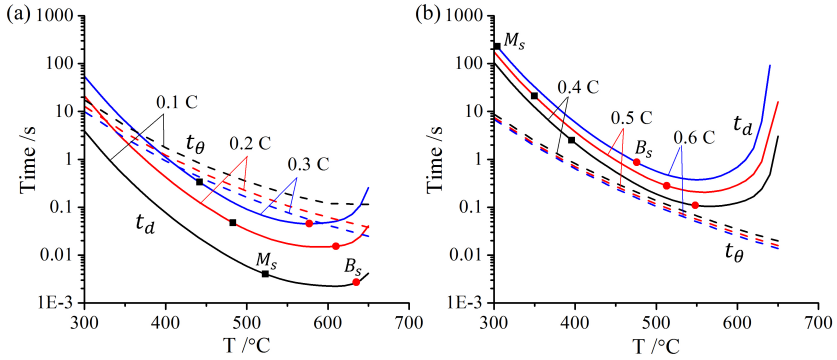


Figure 8: Calculated $t_d$ and $t_\theta$ for plain carbon steel of 0.1-0.6 C wt%, the solid lines are $t_d$, the dash lines are $t_\theta$.

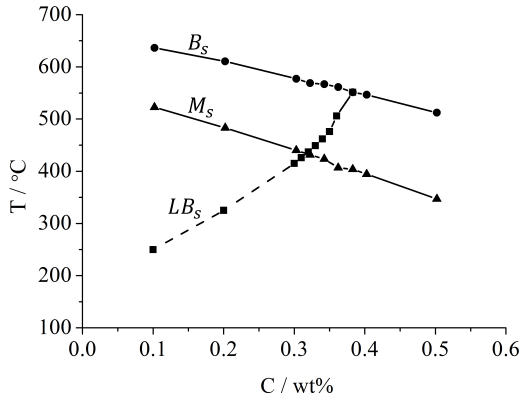


Figure 9: Calculated $LB_s$ temperature for plain carbon steel, with $M_s$ and $B_s$ indicated.

### *5.2. Fe-Mn-Mo-C alloys*

Pickering [42] has systematically studied the effect of carbon on the transition temperature from upper to lower bainite in a series of low alloy Fe-Mn-Mo-C alloys with Mn 0.5 wt% and Mo 0.5 wt%. On applying the model to his data, good agreement is obtained as shown in Fig. 10, although the discrepancy is large at carbon content below 0.2 wt%, but as the calculated transition temperature is below the calculated $M_s$, it becomes invalid as martensite is the predicted phase. The $B_s$ and $M_s$ are calculated following the method of Bhadeshia [43, 44]. In this case, lower bainite is always obtained when carbon content exceeds about 0.3 wt%, this carbon content at the peak of $LB_s$ is lower than that of Fe-C system.

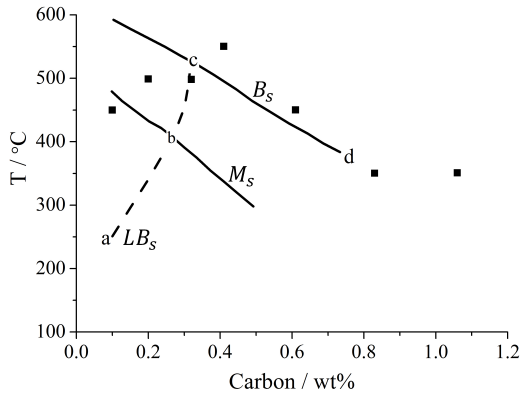


Figure 10: Effect of carbon concentration on the temperature of upper to lower bainite transition in Fe-Mn-Mo-C alloys. Points represent experimentally measured transition temperatures due to Pickering, whereas the curve 'abcd' represents the calculated transition temperature.

### *5.3. Experimental steel*

The effect of carbon on the transition temperatures of the alloy detailed in Table 1 is shown in Fig. 11. Carbon contents below 0.2 wt% show only upper bainite, while carbon content higher than 0.3 wt% gives only lower bainite. There will be transition from upper to lower bainite for carbon contents from 0.21 to 0.26 wt%, and the corresponding $LB_s$ are shown in table 2, an increase in carbon content leads to higher $LB_s$.

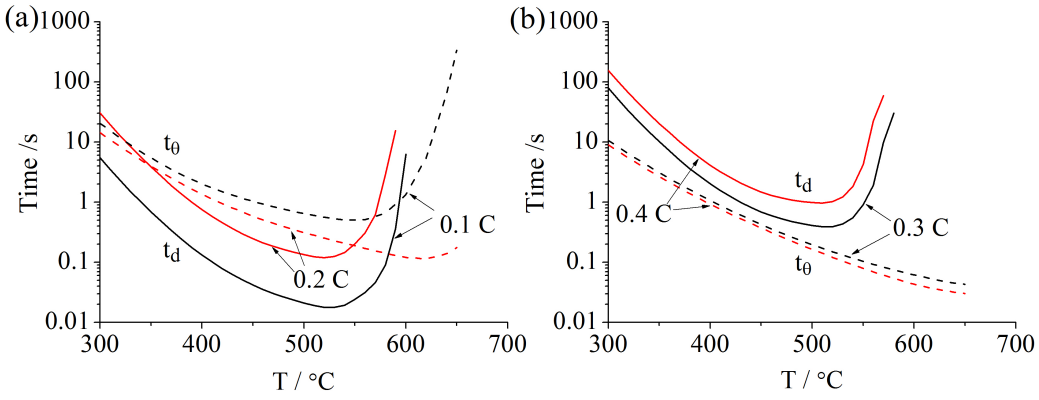


Figure 11: Calculated $t_\theta$ and $t_d$ for the present alloy system with different carbon contents.

Table 2: Lower bainite start temperature for experimental alloy.

| C /wt% | $LB_s$ /°C |
|---|---|
| 0.21 | 355 |
| 0.22 | 367 |
| 0.23 | 378 |
| 0.24 | 388 |
| 0.25 | 402 |
| 0.26 | 420 |
| 0.27 | $\alpha_{LB}$ |
| 0.28 | $\alpha_{LB}$ |
| 0.29 | $\alpha_{LB}$ |

The carbon content at the peak of $LB_s$ calculated for the alloy is lower than that of the Fe-Mn-Mo-C alloys, whose value is lower than that of Fe-C system. This trend agrees with experimental result from Parker [45], who found the peak of transition temperature shifts to low carbon content with the increase of alloying element concentration.

The present steel has a carbon content of 0.224 wt%, which according to the model prediction should have a lower bainite start temperature of 370 °C. TEM micrograph of transformation at 400 °C, 370 °C and 340 °C are shown in Fig. 12. No carbide was found for transformation at 400 °C, while there are carbides in samples transformed at 370 °C and 340 °C. The carbides were confirmed to be cementite by selected area diffraction pattern as shown in the inset of Fig. 12 (b). The microstructure of transformation at 370 °C consist of a mixture of upper and lower bainite, with most carbides found to be in the thick platelets of bainite, as the decarburisation requires more time for thicker platelet, hence the chance for precipitation is larger. The lower bainite may also be formed in the late stage of transformation when the austenite has been enriched with carbon. Pickering has also reported a mixture of upper and lower bainite near the transition temperature [42]. Transformation at 340 °C shows more carbides, even though it is a few degrees below the $M_s$ temperature and the microstructure consists of bainite and martensite, but the decarburisation and precipitation kinetics should be the same as bainite plate, since the bainite plate was initially supersaturated with carbon. So the result is in a broad agreement with the model prediction.

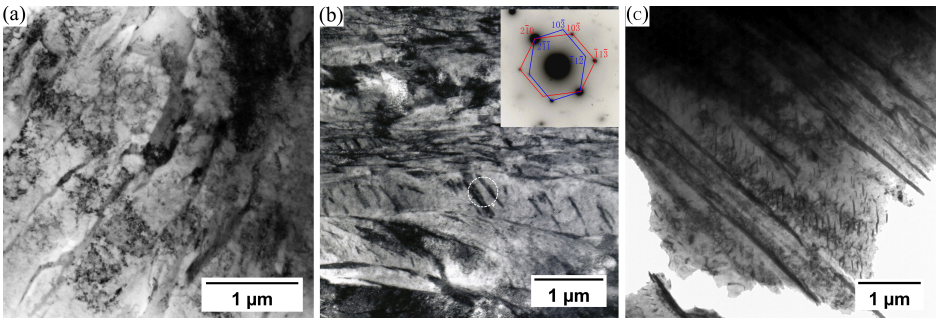


Figure 12: TEM bright field image of transformation at 400 °C, 370 °C and 340 °C for 1 h. (a). 400 °C, (b). 370 °C, the inset is the diffraction pattern from the circled area, the carbides were confirmed to be cementite, zone axes are [351] and [361] for blue and red patterns respectively. (c). 340 °C.

## 6. Summary

A model for the transition from upper to lower bainite has been developed by comparing the time required for decarburising a supersaturated bainite plate and the time for cementite precipitation within the ferrite plate. Good agreement was achieved for Fe-C system and low alloyed Fe-Mn-Mo-C system, broad agreement was reached for a commercial Si-containing multi-component steel. The model predicts that C and Mn favours lower bainite, while Si promotes upper bainite.

The method of calculating the transition temperature nevertheless has the following limitations:

- It is assumed that the composition of the austenite, and hence of the bainite that grows is given by the average in the alloy of interest. However, the austenite enriches in carbon as bainite evolves, so it is possible that initial transformation would be to upper bainite, followed by lower bainite formation when the enrichment is sufficient. This issue has been discussed in detail by Bhadeshia [1, p. 203]; Chang [46] has shown experimentally that a mixture of upper and lower bainite can be obtained when transforming steel at a temperature close to the transition. However, this problem should only be an issue when the transformation conditions are close to the transition temperature, otherwise, the microstructure should be predominantly upper or lower bainitic.

- It is possible to obtain lower bainite with transition carbides of iron, rather than cementite. The procedure for dealing with this is the same as for cementite, but an additional theory would be necessary in order to assess when a thermodynamically more stable cementite is preceded by the transition carbide.

- The bainite plate thickness can be measured using stereological methods such as described in reference [47]; the uncertainty associated with using such data has been determined to be $\pm 10.5\%$ [48].

- We have followed Takahashi and Bhadeshia [2] in setting the fraction of cementite (normalised by the equilibrium fraction) to be 0.01 in predicting the transition temperature. This is because it produces good agreement with data on Fe-C alloys [2]. However, the fraction is arbitrary but the reasoning given in [2] is that the onset of precipitation would quickly retard the partioning of excess carbon over longer distances into the adjacent austenite. We note that the precipitation and partitioning models should strictly be coupled in order to better represent the process.

## 7. References


1. H. K. D. H. Bhadeshia: Bainite in steels: theory and practice: 3rd ed., Leeds, U.K.: Maney Publishing, 2015.

2. M. Takahashi, and H. K. D. H. Bhadeshia: 'Model for transition from upper to lower bainite', *Materials Science and Technology*, 1990, **6**, 592–603.

3. M. Takahashi, and H. K. D. H. Bhadeshia: 'A model for the microstructure of some advanced bainitic steels', *Materials Transactions, JIM*, 1991, **32**, 689–696.

4. Z. Lawrynowicz: 'Transition from upper to lower bainite in Fe-C-Cr steel', *Materials Science and Technology*, 2004, **20**, 1447–1454.

5. M. Azuma, N. Fujita, M. Takahashi, T. Senuma, D. Quidort, and T. Lung: 'Modelling upper and lower bainite transformation in steels', *ISIJ International*, 2005, **45**, 221–228.

6. A. G. Allten, and P. Payson: 'The effect of silicon on the tempering of martensite', *Trans. ASM*, 1953, **45**, 498–532.

7. W. S. Owen: 'The effect of silicon on the kinetics of tempering', *Trans. ASM*, 1954, **46**, 812–829.

8. J. Gordine, and I. Codd: 'The influence of Si up to 1.5 wt% on the tempering of a spring steel', *Journal of the Iron and Steel Institute*, 1969, **207**, 461–467.

9. R. M. Hobbs, G. W. Lorimer, and N. Ridley: 'Effect of silicon on the microstructure of quenched and tempered medium carbon steels', *Journal of the Iron and Steel Institute*, 1972, **210**, 757–764.

10. H. K. D. H. Bhadeshia, and D. V. Edmonds: 'The bainite transformation in a silicon steel', *Metallurgical Transactions A*, 1979, **10A**, 895–907.

11. D. Quidort, and Y. Brechet: 'Isothermal growth kinetics of bainite in 0.5% C steels', *Acta Materialia*, 2001, **49**(20), 4161–4170.

12. E. Kozeschnik, and H. K. D. H. Bhadeshia: 'Influence of silicon on cementite precipitation in steels', *Materials Science and Technology*, 2008, **24**, 343–347.

13. T. Sakum, T. Watanabe, and T. Nishizawa: 'The effect of alloying element on the coarsening behavior of cementite particles in ferrite', *Transactions of the Japan Institute of Metals*, 1980, **21**(3), 159–168.

14. G. Miyamoto, J. C. Oh, K. Hono, T. Furuhara, and T. Maki: 'Effect of partitioning of Mn and Si on the growth kinetics of cementite in tempered Fe-0.6 mass% C martensite', *Acta Materialia*, 2007, **55**, 5027–5038.

15. T. Suzuki, Y. Ono, G. Miyamoto, and T. Furuhara: 'Effects of Si and Cr on bainite microstructure of medium carbon steels', *ISIJ International*, 2010, **50**, 1476–1482.

16. H. K. D. H. Bhadeshia: 'Diffusion of carbon in austenite', *Metal Science*, 1981, **15**, 477–479.

17. H. K. D. H. Bhadeshia: 'Bainite in steels', In: G. W. Lorimer, ed. *Phase Transformations '87*. London, U.K.: Institute of Metals, 1988:309–314.

18. R. W. K. Honeycombe, and H. K. D. H. Bhadeshia: Steels: Microstructure and Properties, 2nd edition: Butterworths-Hienemann, London, 1995.

19. D. M. Goldstein, and L. J. M. (eds): 'Proceedings of the NITINOL heat engine conference': Tech. Rep. NSWC MP 79-441, U.S. Naval Surface Weapons Centre, Maryland, U.S.A., 1978.

20. R. B. McLellan, and W. W. Dunn: 'A quasichemical treatment of interstitial solid solutions: its application to carbon in austenite', *Journal of Physics and Chemistry of Solids*, 1969, **30**, 2631–2637.

21. R. H. Siller, and R. B. McLellan: 'Application of first order mixing statistics to the variation of the diffusivity of carbon in austenite', *Metallurgical Transactions*, 1970, **1**, 985–988.

22. C. S. Smith: 'Microstructure', *Trans. A. S. M.*, 1953, **45**, 533–575.

23. R. Trivedi, and G. M. Pound: 'Effect of concentration dependent diffusion coefficient on the migration of interphase boundaries', *Journal of Applied Physics*, 1967, **38**, 3569–3576.

24. H. K. D. H. Bhadeshia, and L.-E. Svensson: 'Microstructure of submerged arc-weld deposits for high-strength steels', *Journal of Materials Science*, 1989, **24**, 3180–3188.

25. S. S. Babu, K. Hono, and T. Sakuri: 'APFIM studies on martensite tempering of Fe-C-Si-Mn steel', *Applied Surface Science*, 1993, **67**, 321–327.

26. R. C. Thomson, and H. K. D. H. Bhadeshia: 'Atom probe and stem studies of carbide precipitation in 2.25Cr1Mo steel', *Applied Surface Science*, 1993, **67**, 334–341.

27. R. C. Thomson, and M. K. Miller: 'Partitioning of substitutional solute elements during the tempering of martensite in Cr and Mo containing steels', *Applied Surface Science*, 1995, **87-88**, 185–193.

28. R. Thomson, and M. Miller: 'An atom probe study of cementite precipitation in autotempered martensite in an fe mn c alloy', *Applied surface science*, 1996, **94**, 313–319.

29. R. C. Thomson, and M. K. Miller: 'Carbide precipitation in martensite during the early stages of tempering cr-andmo-containing low alloy steels', *Acta materialia*, 1998, **46**, 2203–2213.

30. G. Ghosh, C. E. Campbell, and G. B. Olson: 'Analytical electron microscopy study of paraequilibrium cementite precipitation in ultra-high strength steel', *Metallurgical & Materials Transactions A*, 1999, **30**, 501–512.

31. G. Ghosh, and G. B. Olson: 'Precipitation of paraequilibrium cementite: experiments, thermodynamic and kinetic modelling', *Acta Materialia*, 2002, **50**, 2099–2119.

32. F. G. Caballero, M. K. Miller, S. S. Babu, and C. Garcia-Mateo: 'Atomic scale observations of bainite transformation in a high carbon high silicon steel', *Acta Materialia*, 2007, **55**, 381–390.

33. E. Kozeschnik, and B. Buchmayr: 'MATCALC- a simulation tool for multicomponent thermodynamics, diffusion and phase transformations', In: H. Cerjak, ed. *International Seminar on the Numerical Analysis of Weldability*, vol. 5. London, U.K.: Maney, 1999:349–361.

34. D. J. C. MacKay: 'Practical Bayesian framework of backpropagation networks', *Neural Computation*, 1992, **4**, 448–472.

35. D. J. C. MacKay: 'Bayesian interpolation', *Neural Computation*, 1992, **4**, 415–447.

36. H. K. D. H. Bhadeshia: 'Neural networks and information in materials science', *Statistical Analysis and Data Mining*, 2009, **1**, 296–305.

37. H. K. D. H. Bhadeshia, R. C. Dimitriu, S. Forsik, J. H. Pak, and J. H. Ryu: 'On the performance of neural networks in materials science', *Materials Science and Technology*, 2009, **25**, 504–510.

38. H. K. D. H. Bhadeshia: 'Neural networks in materials science', *ISIJ International*, 1999, **39**, 966–979.

39. S. B. Singh, and H. K. D. H. Bhadeshia: 'Topology of grain deformation', *Materials Science and Technology*, 1998, **15**, 832–834.

40. M. Oka, and H. Okamoto: 'Isothermal transformations in hypereutectoid steels', In: *International Conference on Martensitic Transformations ICOMAT '86*. Tokyo, Japan: Japan Institute of Metals, 1986:271–275.

41. Y. Ohmori, and R. W. K. Honeycombe: 'The isothermal transformation of plain carbon steels', *Supplement to Trans. ISIJ*, 1971, **11**, 1160–1164.

42. F. B. Pickering: 'The structure and properties of bainite in steels', In: *Transformation and hardenability in steels*. Michigan, USA: Climax Molybdenum Co., 1967:109–132.

43. H. K. D. H. Bhadeshia: 'A thermodynamic analysis of isothermal transformation diagrams', *Metal Science*, 1982, **16**, 159–165.

44. H. K. D. H. Bhadeshia: 'Software for transformations in steels': http://www.msm.cam.ac.uk/map/steel/programs/mucg46-b.html, 1982.

45. E. R. Parker: 'Interrelations of compositions, transformation kinetics morphology and mechanical properties of alloy steels', *Metallurgical Transactions A*, 1977, **8A**, 1025–1042.

46. L. C. Chang: 'Bainite transformation temperatures in high-silicon steels', *Metallurgical & Materials Transactions A*, 1999, **30**, 909–916.

47. L. C. Chang, and H. K. D. H. Bhadeshia: 'Austenite films in bainitic microstructures', *Materials Science and Technology*, 1995, , 874–881.

48. S. B. Singh, and H. K. D. H. Bhadeshia: 'Estimation of bainite plate-thickness in low-alloy steels', *Materials Science & Engineering A*, 1998, **245**, 72–79.